Journal of Zhejiang University-SCIENCE A (Applied Physics & Engineering) *2024 25(8):605-617*
www.jzus.zju.edu.cn; www.springer.com/journal/11582
E-mail: jzus_a@zju.edu.cn

Research Article
https://doi.org/10.1631/jzus.A2300517

Frequency-domain analysis of fluid-structure interaction in aircraft hydraulic pipeline systems: numerical and experimental studies

Yang DENG[1], Zongxia JIAO[1,2,3,4,5], Yuanzhi XU[1,2,3,4,5]✉

[1]*School of Automation Science and Electrical Engineering, Beihang University, Beijing 100191, China*
[2]*Research Institute for Frontier Science, Beihang University, Beijing 100191, China*
[3]*Key Laboratory of Advanced Airborne Systems, Beihang University, Beijing 100191, China*
[4]*Ningbo Institute of Technology, Beihang University, Ningbo 315800, China*
[5]*Tianmushan Laboratory, Hangzhou 310023, China*

Abstract: The fluid-structure interaction (FSI) in aircraft hydraulic pipeline systems is of great concern because of the damage it causes. To accurately predict the vibration characteristic of long hydraulic pipelines with curved segments, we studied the frequency-domain modeling and solution method for FSI in these pipeline systems. Fourteen partial differential equations (PDEs) are utilized to model the pipeline FSI, considering both frequency-dependent friction and bending-flexibility modification. To address the numerical instability encountered by the traditional transfer matrix method (TMM) in solving relatively complex pipelines, an improved TMM is proposed for solving the PDEs in the frequency domain, based on the matrix-stacking strategy and matrix representation of boundary conditions. The proposed FSI model and improved solution method are validated by numerical cases and experiments. An experimental rig of a practical hydraulic system, consisting of an aircraft engine-driven pump, a Z-shaped aero-hydraulic pipeline, and a throttle valve, was constructed for testing. The magnitude ratio of acceleration to pressure is introduced to evaluate the theoretical and experimental results, which indicate that the proposed model and solution method are effective in practical applications. The methodology presented in this paper can be used as an efficient approach for the vibrational design of aircraft hydraulic pipeline systems.

Key words: Fluid-structure interaction (FSI); Frequency-domain analysis; Aircraft hydraulic pipeline; Pipeline vibration; Transfer matrix method (TMM)

1 Introduction

Hydraulic systems are widely used in aircraft due to their advantages of high power-to-weight ratio and response speed. Pipeline systems are utilized to transmit hydraulic power from the pump to each actuator, such as the rudder and brake system (Wang et al., 2015). The reliable operation of hydraulic pipelines is critical to flight safety. However, the pressure pulsations generated by aero-hydraulic pumps excite pipe vibrations, which can cause damage to the entire pipeline system in the form of cracked pipe walls, damaged pipe joints, or torn brackets (Gao et al., 2021). Additionally, due to the large number of curved pipe segments within the system, fluid-structure interaction (FSI) behavior is noticeable in aircraft hydraulic pipeline systems. Unlike short-term events involving fluid transients, pump-excited long-term hydraulic events may involve acoustic resonance and structural fatigue (Tijsseling, 2019), and thus more focus should be put on frequency-domain analysis. This was the impetus behind our study of FSI in aircraft hydraulic pipelines.

The behavior of pipeline FSI can be described using first-order linear partial differential equations (PDEs) that have evolved from the four-equation model to the 14-equation model (Wiggert and Tijsseling, 2001; Li et al., 2015). To be specific, Skalak (1956) extended the classical two-equation water-hammer theory to a simplified four-equation model that considered the Poisson coupling. Davidson and Smith (1969) developed an eight-equation model accounting for axial motion and in-plane flexural motion in curved

✉ Yuanzhi XU, yz.xu.ac@gmail.com
Yuanzhi XU, https://orcid.org/0009-0000-3315-6755

Received Oct. 11, 2023; Revision accepted Dec. 23, 2023;
Crosschecked July 25, 2024

pipelines, and the theory was validated by means of a curved pipe with a free open end and pulse excitation at the inlet port. Subsequently, Davidson and Smith (1972) expanded the method to non-planar pipelines by introducing a variable vector with 14 elements for modeling 3D pipes. Wiggert et al. (1987) presented the 14-equation model of FSI for a straight liquid pipe, based on the Timoshenko beam theory. In summary, the four-equation model can only describe the axial motion of the pipe, the eight-equation model adds the transverse motion of the pipe in one plane, and the 14-equation model can describe the transverse motion of the pipe in two planes as well as its axial torsional motion. The 14-equation model is suitable for the FSI in 3D liquid pipelines. In practical fluid systems, the friction coupling needs to be considered in order to describe the dynamic behavior of hydraulic pipelines more accurately. Jiao et al. (1999) considered the influence of frequency-dependent friction based on Zielke (1968)'s model. Friction was also considered in the FSI model designed by Brown and Tentarelli (2001). As mentioned above, curved pipes are very common in aircraft hydraulic pipelines. Lesmez et al. (1990) and Li et al. (2022) modeled curved pipes with an equivalent series of straight pipe sections, each of which was placed at an angle. The model accuracy depends on the number of straight segments used. de Jong (1994), as well as Brown and Tentarelli (2001), proposed the 14 differential equations for curved pipes, which is an analytical representation model. In this paper, in order to obtain more accurate predictions and more comprehensive results for aircraft hydraulic pipeline systems, the 14-PDE FSI model is used to describe both straight and curved pipes, while taking into consideration the friction term. In addition, for the stiffness of curved pipes, Vigness (1943) and Pardue and Vigness (1951) found experimentally that the longitudinal stress tended to distort the cross-sectional shapes in the curved sections. Therefore, a flexibility modification needed to be introduced into the bending equations in order to describe the intrinsic properties of curved sections accurately; this was also reported by de Jong (1994).

In terms of frequency-solution methods for FSI in liquid pipeline systems, the transfer matrix method (TMM) has been widely employed due to its high computational efficiency and ease of programming. Lesmez et al. (1990) used the Laplace transform and TMM to solve the pipeline FSI problem, and the method was validated experimentally on a U-shaped pipe with a shaker. Inspired by the method of characteristics (MOC), Zhang et al. (1999) proposed a decoupling approach to solve the frequency equations obtained by the Laplace transform. Li et al. (2002) extended Zhang et al. (1999)'s method by reorganizing the boundary matrix and system-transfer matrix into a global matrix to solve the FSI problem in a multi-section pipeline. Yang et al. (2004) also applied this solution method to investigate FSI in pipelines with multi-span pipes. Liu and Li (2011) investigated FSI in a liquid pipe based on Lesmez et al. (1990)'s frequency-domain method. Li et al. (2014) solved the FSI problem in liquid pipes with TMM, based on Zhang et al. (1999)'s method. Ouyang et al. (2012a, 2012b) calculated an aircraft pipeline's modes based on the TMM, performing eight-equation modeling of the curved pipe and analyzing the effects with different bending curvatures. Xu et al. (2014) investigated the frequency-domain solution of FSI in liquid-filled pipes, based on a complex pipe with multiple branches and supports. Gao et al. (2016) introduced a model-reduction approach that used the finite element method (FEM) for vibration analysis of aero-hydraulic pipelines; the proposed method further reduced the time required for calculation. Guo et al. (2022a, 2022b, 2022c, 2022d, 2022e, 2023) studied the vibration characteristics of L-shaped pipes with supports and parallel pipes with fluid and structure base excitation. Ji et al. (2023) investigated the stress response in a liquid pipe system using a combination of the FEM and TMM. However, numerical instability was reported by Kwong and Edge (1996). As pipeline length and complexity increase, rounding errors and computational instability may arise due to the ill-conditioned matrices in the TMM solution process. Aircraft hydraulic pipelines in particular may have more instability problems due to the complexity of their configuration. To address this problem, we propose an improved TMM in this paper, which is based on the matrix-stacking method and matrix-description method of boundary conditions.

With regard to the published FSI experiments, most of them deal with simple configurations and boundary conditions, and FSI experiments on practical hydraulic systems are rare (Jiao et al., 1999; Brown and Tentarelli, 2001; Tentarelli and Brown, 2001). The reviews (Li et al., 2015; Ferras et al., 2018)

present a large amount of literature related to computational methods and only a few papers that discuss practical experimental systems for validation.

This paper is organized as follows: The 14-PDE FSI model considering frequency-dependent friction and bending-flexibility modification is presented in Section 2. In Section 3, an improved transfer-matrix algorithm is proposed, to overcome the problem of computational instability. The numerical cases of a single straight pipe and a curved pipeline are studied in Section 4. Finally, in Section 5, an experimental rig of aero-hydraulic piping system is established, and the FSI experiments indexed by fluid pressure and pipe acceleration are carried out.

2 Partial differential 14-equation model for FSI of hydraulic pipes

2.1 Fourteen-equation FSI model of a straight pipe

A differential element of a straight hydraulic pipe is shown in Fig. 1, where p and v_f represent the fluid pressure and velocity, u_x, u_y, u_z and f_x, f_y, f_z denote the displacements and forces of pipe wall along the three linear directions, and φ_x, φ_y, φ_z and m_x, m_y, m_z denote the angles and moments at three torsional directions, respectively. The length of the microelement is represented by dz. Fourteen variables were introduced to describe the dynamic behavior of the pipe. Based on the variable coordinate definitions between both sides of the differential element, equilibrium equations and motion equations can be derived, resulting in a set of 14 one-order PDEs (Wiggert et al., 1987) that describe the FSI behavior of the hydraulic pipe.

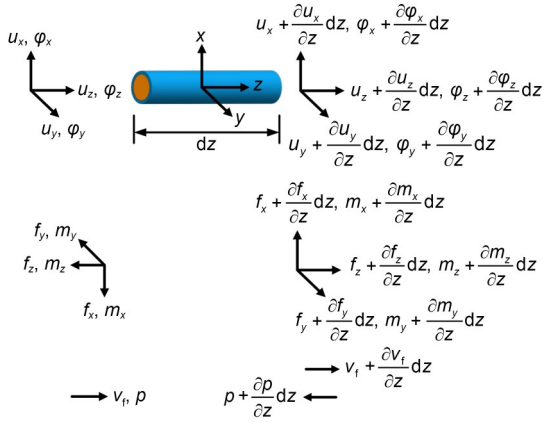

Fig. 1 Differential element of a straight hydraulic pipe

It is important to note that, unlike the case of normal fluid-conveying pipes, dynamic friction needs to be considered, as hydraulic fluids have a higher viscosity than water systems. Additionally, the operating frequency of the hydraulic system, which is primarily influenced by the flow ripple of the pump, falls within a relatively high range where dynamic friction is frequency-dependent.

The axial force equilibria considering the friction effects for the fluid and pipe wall are shown in Fig. 2, where F_f denotes the friction force, and r represents the inner radius of the pipe. The force equilibrium equations for the fluid and pipe wall can be described as

$$pA_f-\left(p+\frac{\partial p}{\partial z}\mathrm{d}z\right)A_f-F_f=\rho_f A_f \mathrm{d}z\frac{\partial v_f}{\partial t}, \tag{1}$$

$$\left(f_z+\frac{\partial f_z}{\partial z}\mathrm{d}z\right)-f_z+F_f=\rho_p A_p \mathrm{d}z\frac{\partial u_z}{\partial t}, \tag{2}$$

where A_f and A_p denote the cross-sectional areas of fluid and pipe wall, and ρ_f and ρ_p represent the densities of fluid and pipe wall, respectively. t is the time.

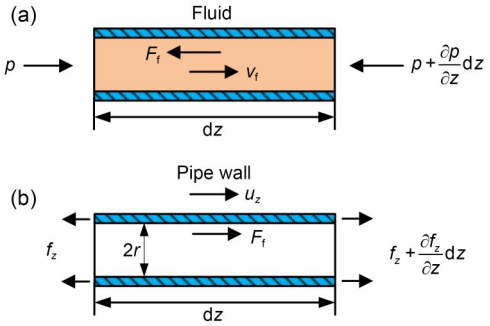

Fig. 2 Force equilibria in the axial direction: (a) force equilibrium of fluid; (b) force equilibrium of pipe wall

Subsequently, the widely used Zielke (1968)'s frequency-independent friction model is brought in, as

$$F_f=2\pi r\tau_0 \mathrm{d}z, \tag{3}$$

where τ_0 represents the shear friction at the pipe wall.

For the frequency-domain description of τ_0, Zielke (1968) derived a fluid-friction model using the Bessel function:

$$\tilde{\tau}_0(s)=\frac{\rho_f r}{\vartheta_1\left(\mathrm{j}r\sqrt{s/\zeta_f}-2\right)}sv_f(s), \tag{4}$$

where the superscript '~' denotes Laplace-transformed variables, s is the Laplace operator, j is equal to $\sqrt{-1}$, ζ_f is the fluid viscosity, and $\vartheta_1(x)=x\dfrac{J_0(x)}{J_1(x)}$, with $J_0(x)$ and $J_1(x)$ being zero and first-order Bessel functions, respectively.

By substituting Eq. (3) into Eqs. (1) and (2), the equations can be rewritten as

$$\frac{1}{\rho_f}\frac{\partial p}{\partial z}+\frac{\partial v_f}{\partial t}+\frac{2\tau_0}{r\rho_f}=0, \tag{5}$$

$$\frac{\partial f_z}{\partial z}-\rho_p A_p\frac{\partial \dot{u}_z}{\partial t}+2\pi r\tau_0=0. \tag{6}$$

The complete FSI model of the straight pipe, considering the dynamic friction effect, is shown in Section S1 of the electronic supplementary materials (ESM), and is suitable for aircraft hydraulic pipeline systems. The appendices mentioned in this paper are available in the ESM.

2.2 Fourteen-equation FSI model of curved pipe

A series of short straight segments connected by miter bends can be an equivalent representation of a curved pipe. However, this is ultimately a relatively approximate model, and its accuracy is limited by the number of segments. In order to achieve an accurate analytical representation of the curved pipe model rather than a mechanistic approximation, we here describe the curved pipe using the PDE model. The differential element for the curved pipe is illustrated in Fig. 3, where dθ and dl represent the angle and length of the microelement, respectively, and R denotes the radius of the curvature.

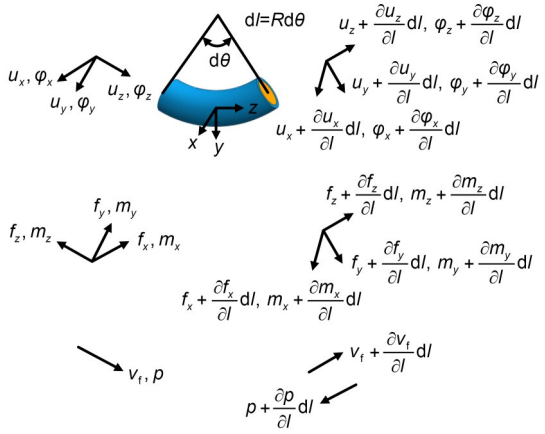

Fig. 3 Differential element of a curved pipe

In contrast to straight pipes, it is necessary to introduce a flexibility modification factor when dealing with curved pipes because the longitudinal stress tends to distort the cross-sectional shapes. The bending equations for the curved pipe in the y-z and x-z planes are

$$\frac{\partial m_y}{\partial t}-\kappa_E EI_p\left(\frac{\partial \dot{\varphi}_y}{\partial l}-\frac{\dot{\varphi}_z}{R}\right)=0, \tag{7}$$

$$\frac{\partial m_x}{\partial t}-\kappa_E EI_p\frac{\partial \dot{\varphi}_x}{\partial l}=0, \tag{8}$$

where E denote Young's modulus of the pipe wall, and I_p denotes the flexure moment of inertia. As proposed by de Jong (1994), the flexibility modification factor κ_E is $e_pR/(1.65r^2)$, where e_p denotes the thickness of pipe. The 14 PDEs for the curved pipe are presented in Section S2 of the ESM.

3 Frequency solution for pipeline FSI with the TMM

3.1 TMM for FSI of hydraulic pipes

The 14 PDEs presented in Section 2 can be written in matrix form as

$$\boldsymbol{A}(\partial/\partial t)\boldsymbol{\Phi}(z,\ t)+\boldsymbol{B}(\partial/\partial z)\boldsymbol{\Phi}(z,\ t)+\boldsymbol{C}\boldsymbol{\Phi}(z,\ t)=\boldsymbol{0}, \tag{9}$$

where $\boldsymbol{A}$, $\boldsymbol{B}$, and $\boldsymbol{C}$ are coefficient matrices and $\boldsymbol{\Phi}$ denotes the vector of system variables.

The state vector of pipe can be defined as

$$\boldsymbol{\Phi}(z,\ t)=(v_f\ p_f\ \dot{u}_z\ f_z\ \dot{u}_y\ f_y\ \dot{\varphi}_x\ m_x\ \dot{u}_x\ f_x\ \dot{\varphi}_y\ m_y\ \dot{\varphi}_z\ m_z)^{\mathrm{T}}. \tag{10}$$

Eq. (9) can be Laplace-transformed into the ordinary differential equation as

$$s\boldsymbol{A}\tilde{\boldsymbol{\Phi}}(z,\ s)+\boldsymbol{B}(\partial/\partial z)\tilde{\boldsymbol{\Phi}}(z,\ s)+\boldsymbol{C}\tilde{\boldsymbol{\Phi}}(z,\ s)=\boldsymbol{0}. \tag{11}$$

Then, Eq. (11) can be rearranged as

$$(\partial/\partial z)\tilde{\boldsymbol{\Phi}}(z,\ s)=\boldsymbol{A}^*\tilde{\boldsymbol{\Phi}}(z,\ s), \tag{12}$$

where $\boldsymbol{A}^*=-\boldsymbol{B}(s\boldsymbol{A}+\boldsymbol{C})$.

By integrating Eq. (12) from $z=z_0$ to $z=z_L$, as illustrated in Fig. 4, one can obtain

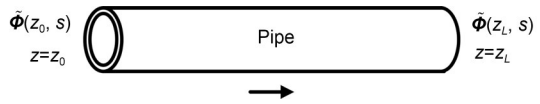

Fig. 4 Straight hydraulic pipe

$$\tilde{\boldsymbol{\Phi}}(z_L, s) = \boldsymbol{M}(z_L - z_0, s)\tilde{\boldsymbol{\Phi}}(z_0, s), \tag{13}$$

where

$$\boldsymbol{M}(z_L - z_0, s) = \mathrm{e}^{\boldsymbol{A}^*(z_L - z_0)} \tag{14}$$

is the transfer matrix of the hydraulic pipe, and L denotes the total length of the pipe.

The boundary conditions at both ends of the pipe can also be described using matrix form. Zhang et al. (1999) and Xu et al. (2014) proposed these boundary conditions as

$$\boldsymbol{D}_0(s)\tilde{\boldsymbol{\Phi}}(z_0, s) = \boldsymbol{E}_0(s), \tag{15}$$
$$\boldsymbol{D}_L(s)\tilde{\boldsymbol{\Phi}}(z_L, s) = \boldsymbol{E}_L(s), \tag{16}$$

where $\boldsymbol{D}_0(s)$ and $\boldsymbol{E}_0(s)$ represent the boundary matrices for the left pipe end, and $\boldsymbol{D}_L(s)$ and $\boldsymbol{E}_L(s)$ denote the boundary matrices for the right pipe end.

3.2 Improved TMM for the pipeline system

When solving a hydraulic pipeline system, the system transfer matrix needs to be introduced into the solution process. For the longer pipeline system including more pipe segments (shown in Fig. 5), the system transfer matrix can be obtained by

$$\begin{aligned}\boldsymbol{M}_{\text{system}}(L, s) = {}& \boldsymbol{M}_N(L_N, s)\boldsymbol{M}_{N-1}(L_{N-1}, s)\cdots \\ & \boldsymbol{M}_3(L_3, s)\boldsymbol{M}_2(L_2, s)\boldsymbol{M}_1(L_1, s),\end{aligned} \tag{17}$$

where L_i (i=1, 2, ⋯, N) denotes the length of the ith section of pipe.

However, as the complexity of the pipeline increases, the condition number of the system transfer matrix (defined as the ratio between its largest and smallest singular values) also increases rapidly because the pipe transfer matrix contains elements that are exponential with respect to the length of the pipe and the frequency of the vibration. As a result, the unknown variables are extremely sensitive to quantization and rounding errors in the ill-conditioned system transfer matrix. Thus, the solution of frequency response will be unstable.

Inspired by the method developed by Kwong and Edge (1996), we propose an improved TMM for solving the issue of computational instability, which combines the ideas of matrix representation of boundary conditions and stacking of transfer matrices. The proposed method has the advantage of being simple, intuitive, and easy to implement programmatically. As depicted in Fig. 5, the variable relationship of segments in the pipeline system can be described by the transfer matrix as

$$\tilde{\boldsymbol{\Phi}}(z_1, s) = \boldsymbol{M}_1(L_1, s)\tilde{\boldsymbol{\Phi}}(z_0, s), \tag{18}$$
$$\tilde{\boldsymbol{\Phi}}(z_2, s) = \boldsymbol{M}_2(L_2, s)\tilde{\boldsymbol{\Phi}}(z_1, s), \tag{19}$$
$$\tilde{\boldsymbol{\Phi}}(z_3, s) = \boldsymbol{M}_3(L_3, s)\tilde{\boldsymbol{\Phi}}(z_2, s), \tag{20}$$
$$\tilde{\boldsymbol{\Phi}}(z_4, s) = \boldsymbol{M}_4(L_4, s)\tilde{\boldsymbol{\Phi}}(z_3, s), \tag{21}$$
$$\tilde{\boldsymbol{\Phi}}(z_L, s) = \boldsymbol{M}_N(L_N, s)\tilde{\boldsymbol{\Phi}}(z_{N-1}, s). \tag{22}$$

Then, based on the matrix-stacking strategy, Eqs. (18)–(22) can be rewritten as Eq. (23).

$$\begin{bmatrix} \boldsymbol{M}_1(L_1,s) & -\boldsymbol{I} & \boldsymbol{0} & \boldsymbol{0} & \boldsymbol{0} & \cdots & \boldsymbol{0} & \boldsymbol{0} \\ \boldsymbol{0} & \boldsymbol{M}_2(L_2,s) & -\boldsymbol{I} & \boldsymbol{0} & \boldsymbol{0} & \cdots & \boldsymbol{0} & \boldsymbol{0} \\ \boldsymbol{0} & \boldsymbol{0} & \boldsymbol{M}_3(L_3,s) & -\boldsymbol{I} & \boldsymbol{0} & \cdots & \boldsymbol{0} & \boldsymbol{0} \\ \boldsymbol{0} & \boldsymbol{0} & \boldsymbol{0} & \boldsymbol{M}_4(L_4,s) & -\boldsymbol{I} & \cdots & \boldsymbol{0} & \boldsymbol{0} \\ \vdots & \vdots & \vdots & \vdots & \vdots & \ddots & \vdots & \vdots \\ \boldsymbol{0} & \boldsymbol{0} & \boldsymbol{0} & \boldsymbol{0} & \boldsymbol{0} & \cdots & \boldsymbol{M}_N(L_N,s) & -\boldsymbol{I} \end{bmatrix} \begin{bmatrix} \tilde{\boldsymbol{\Phi}}(z_0, s) \\ \tilde{\boldsymbol{\Phi}}(z_1, s) \\ \tilde{\boldsymbol{\Phi}}(z_2, s) \\ \vdots \\ \tilde{\boldsymbol{\Phi}}(z_{N-1}, s) \\ \tilde{\boldsymbol{\Phi}}(z_L, s) \end{bmatrix} = \begin{bmatrix} \boldsymbol{0} \\ \boldsymbol{0} \\ \boldsymbol{0} \\ \boldsymbol{0} \\ \vdots \\ \boldsymbol{0} \end{bmatrix}. \tag{23}$$

The boundary conditions at both ends of the pipe can be written as

$$\begin{bmatrix} \boldsymbol{D}_0(s) & \boldsymbol{0} \\ \boldsymbol{0} & \boldsymbol{D}_L(s) \end{bmatrix} \begin{bmatrix} \tilde{\boldsymbol{\Phi}}(z_0, s) \\ \tilde{\boldsymbol{\Phi}}(z_L, s) \end{bmatrix} = \begin{bmatrix} \boldsymbol{E}_0(s) \\ \boldsymbol{E}_L(s) \end{bmatrix}. \tag{24}$$

Thus, the global equation can be obtained by combining Eqs. (23) and (24) together as

$$\boldsymbol{D}^*(s)\tilde{\boldsymbol{\Phi}}^*(s) = \boldsymbol{E}^*(s). \tag{25}$$

Finally, the unknown variables can be obtained by

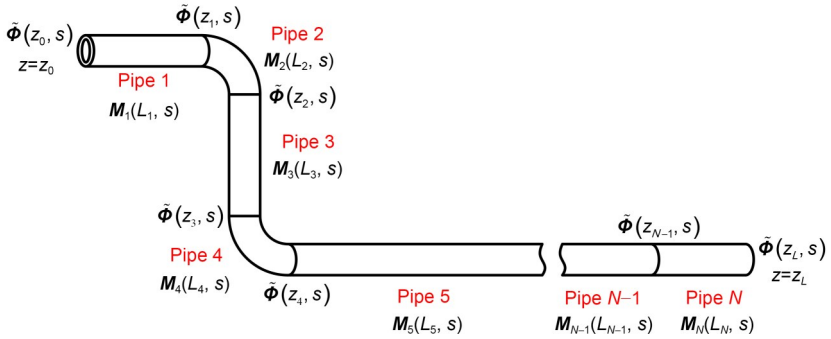

Fig. 5 A serial multi-pipe system

$$\tilde{\boldsymbol{\Phi}}^*(s) = \boldsymbol{D}^*(s)^{-1}\boldsymbol{E}^*(s), \tag{26}$$

$$\boldsymbol{D}^*(s) = \begin{bmatrix} \boldsymbol{D}_0(s) & \boldsymbol{0} & \boldsymbol{0} & \boldsymbol{0} & \boldsymbol{0} & \cdots & \boldsymbol{0} & \boldsymbol{0} \\ \boldsymbol{M}_1(L_1, s) & -\boldsymbol{I} & \boldsymbol{0} & \boldsymbol{0} & \boldsymbol{0} & \cdots & \boldsymbol{0} & \boldsymbol{0} \\ \boldsymbol{0} & \boldsymbol{M}_2(L_2, s) & -\boldsymbol{I} & \boldsymbol{0} & \boldsymbol{0} & \cdots & \boldsymbol{0} & \boldsymbol{0} \\ \boldsymbol{0} & \boldsymbol{0} & \boldsymbol{M}_3(L_3, s) & -\boldsymbol{I} & \boldsymbol{0} & \cdots & \boldsymbol{0} & \boldsymbol{0} \\ \boldsymbol{0} & \boldsymbol{0} & \boldsymbol{0} & \boldsymbol{M}_4(L_4, s) & -\boldsymbol{I} & \cdots & \boldsymbol{0} & \boldsymbol{0} \\ \vdots & \vdots & \vdots & \vdots & \vdots & \ddots & \vdots & \vdots \\ \boldsymbol{0} & \boldsymbol{0} & \boldsymbol{0} & \boldsymbol{0} & \boldsymbol{0} & \cdots & \boldsymbol{M}_N(L_N, s) & -\boldsymbol{I} \\ \boldsymbol{0} & \boldsymbol{0} & \boldsymbol{0} & \boldsymbol{0} & \boldsymbol{0} & \cdots & \boldsymbol{0} & \boldsymbol{D}_L(s) \end{bmatrix}, \tag{27}$$

$$\tilde{\boldsymbol{\Phi}}^*(s) = \left[\tilde{\boldsymbol{\Phi}}(z_0, s) \quad \tilde{\boldsymbol{\Phi}}(z_1, s) \quad \tilde{\boldsymbol{\Phi}}(z_2, s) \quad \tilde{\boldsymbol{\Phi}}(z_3, s) \quad \tilde{\boldsymbol{\Phi}}(z_4, s) \quad \cdots \quad \tilde{\boldsymbol{\Phi}}(z_{N-1}, s) \quad \tilde{\boldsymbol{\Phi}}(z_L, s)\right]^{\mathrm{T}}, \tag{28}$$

$$\boldsymbol{E}^*(s) = [\boldsymbol{E}_0(s) \quad \boldsymbol{0} \quad \boldsymbol{0} \quad \boldsymbol{0} \quad \boldsymbol{0} \quad \cdots \quad \boldsymbol{0} \quad \boldsymbol{E}_L(s)]^{\mathrm{T}}. \tag{29}$$

4 Numerical case studies

4.1 Case for FSI of a straight pipe

First, we used the fluid-filled straight pipe shown in Fig. 6 as a numerical example to verify the FSI solution method. The experiment was carried out at Dundee University, UK (Tijsseling, 1996). The pipe was suspended from flexible ropes at both ends and kept horizontal, and then the left end of the pipe was subjected to axial impact from a steel rod. The mass of the plug at the left pipe end was 1.312 kg, and the mass of the cap at the right end was 0.3258 kg. The fluid mass density was 999 kg/m^3 and the bulk modulus was 2.14 GPa. The detailed geometric and material parameters of the pipe are listed in Table 1.

In order to provide more comprehensive validation of the results calculated by the TMM, we also employed the FEM to calculate the frequency response. Harmonic acoustic analysis was carried out using ANSYS software; the fluid and structural domains were divided into a co-nodal mesh and the FSI surface was defined. Then the TMM and FEM calculation results of the pressure and axial acceleration responses at both ends could be obtained, as shown in Fig. 7. Specifically, Figs. 7a and 7b depict pressure

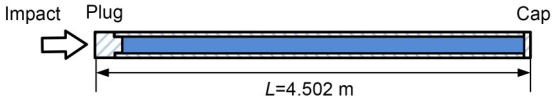

Fig. 6 Geometric diagram of the Dundee straight liquid pipe

Table 1 Parameters of the Dundee straight pipe

Parameter	Value
Mass density (kg/m^3)	7985
Young's modulus (GPa)	168
Shear modulus (GPa)	65.1
Pipe thickness (mm)	3.945
Inter radius (mm)	26.01
Poisson's ratio	0.29

responses on the left and right sides, respectively, while Figs. 7c and 7d illustrate the axial acceleration responses. The frequency response curves show that TMM and FEM exhibited the same trends, which indicated that the two different frequency-domain methods could be verified against each other. The modal frequencies obtained from the experiment, TMM, and FEM are listed in Table 2, which demonstrates the high accuracy achieved by proposed numerical methods.

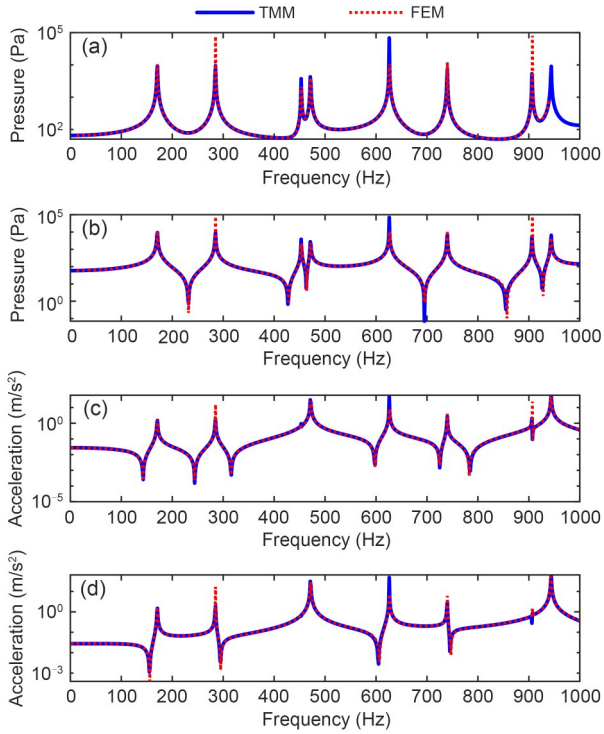

Fig. 7 Pressure and acceleration responses of the Dundee straight pipe at both ends: (a) pressure response at left end; (b) pressure response at right end; (c) acceleration response at left end; (d) acceleration response at right end

Table 2 Modal frequencies of experiment and calculation for the Dundee straight pipe

Experiment frequency (Hz)	TMM		FEM	
	Frequency (Hz)	Error (%)	Frequency (Hz)	Error (%)
173	171	1.16	171	1.16
289	285	1.38	285	1.38
459	453	1.31	454	1.09
485	472	2.68	472	2.68
636	626	1.57	627	1.42
750	740	1.33	740	1.33
918	906	1.31	907	1.20
968	944	2.48	944	2.48

4.2 Case for FSI of a pipeline system with a curved segment

We used a Dundee L-shaped pipe (Tijsseling, 1996) containing two straight pipes and one curved segment to validate the solution method for the cascaded pipe. The geometric parameters of the pipeline are presented in Fig. 8. Similar to the straight pipe, it was suspended by ropes and impacted axially at the left side by the steel rod.

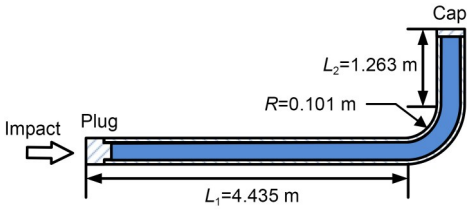

Fig. 8 Geometric diagram of the Dundee L-shaped liquid pipe

The acceleration frequency response results for both ends, as obtained by conventional TMM, are depicted in Figs. 9 and 10. There is a good congruency between the TMM and FEM results, especially from 0 to 500 Hz. However, the instability of TMM, a noise-like curve, is noticeable in the higher frequency range.

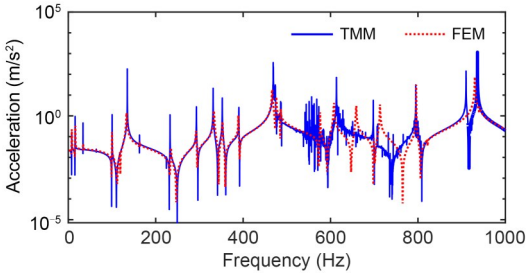

Fig. 9 Axial acceleration responses at the left end of the L-shaped pipe obtained by TMM and FEM

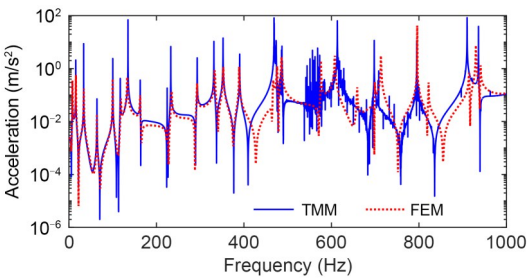

Fig. 10 Axial acceleration responses at the right end of the L-shaped pipe obtained by TMM and FEM

To address the instability problem described above, we utilized the improved TMM proposed in Section 3.2 by stacking the transfer matrix of the divided segments. The relatively long straight pipe segments should be divided into shorter segments to obtain a better instability-suppression effect. Then, the final solution can be obtained; the acceleration responses at both ends determined by improved TMM and FEM are shown in Figs. 11 and 12, demonstrating the effective suppression of instability issues. Modal frequencies of simulation and experiment are listed in Table 3, with a maximum error of 11.11% and minimum error of 0.74%.

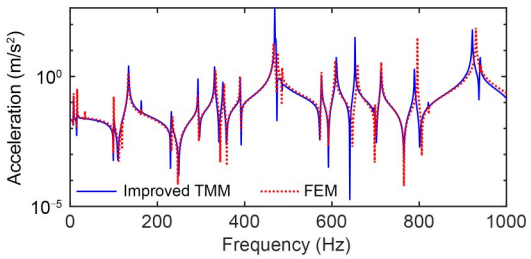

Fig. 11 Axial acceleration responses at the left end of the L-shaped pipe obtained by improved TMM and FEM

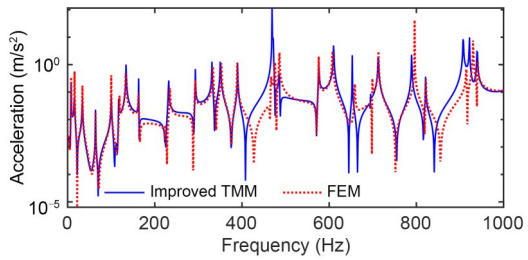

Fig. 12 Axial acceleration responses at the right end of the L-shaped pipe obtained by improved TMM and FEM

5 Experimental validation

5.1 Test rig of aero hydraulic pipeline system with valve

On the basis of successful calculations of straight and curved pipe configurations, we proceeded to validate the theoretical method proposed in this study experimentally; for this, we used a Z-shaped hydraulic pipeline system equipped with an aircraft engine-driven pump (EDP) and a throttle valve. The hydraulic schematic diagram of the test rig is shown in Fig. 13a, and the pump and Z-shaped pipeline are shown in Figs. 13b and 13c, respectively. A pressure sensor was installed at the inlet of the pipe and an accelerometer was positioned in the middle of pipe L_2 to measure the in-plane lateral vibration. The two ends of the pipeline were mounted on rigid blocks which were treated as fixed constraints. The blocks were hydraulic manifolds made of steel, and were mounted on the test bench. As the combined mass of both blocks was over 90 kg, these supports were considered to be rigid. The pipe was connected to the blocks by flanges which were secured by four bolts, thus maintaining high rigidity at the inlet and outlet connections.

Table 3 Modal frequencies of experiment and calculation for the Dundee L-shaped pipeline

Experiment frequency (Hz)	Improved TMM		FEM	
	Frequency (Hz)	Error (%)	Frequency (Hz)	Error (%)
9	8	11.11	8	11.11
17	16	5.88	16	5.88
35	34	2.86	34	2.86
66	64	3.03	64	3.03
104	100	3.85	100	3.85
124	118	4.84	119	4.03
136	135	0.74	133	2.21
168	163	2.98	163	2.98
231	225	2.60	224	3.03
239	233	2.51	235	1.67
303	293	3.30	293	3.30
346	331	4.34	333	3.76
361	352	2.49	353	2.22
401	390	2.74	389	2.99
473	469	0.85	467	1.27
483	474	1.86	476	1.45
499	488	2.20	486	2.61

Details of the instrument parameters used in this experimental setup are listed in Table 4. The configuration for the Z-shaped pipeline is illustrated in Fig. 14. The pipeline in the experiment was excited by the fluid pulsation induced by the hydraulic pump. The pulsating pressure was detected by pressure sensors at the inlet of the pipeline. The liquid used in the experiment was hydraulic oil. All material and geometric properties are presented in Table 5.

5.2 FSI modeling and solution

The Z-shaped pipeline, which consisted of two curved pipe sections, exhibited greater complexity than the L-shaped pipeline. Based on the improved TMM proposed in Section 3.2, we were able to obtain

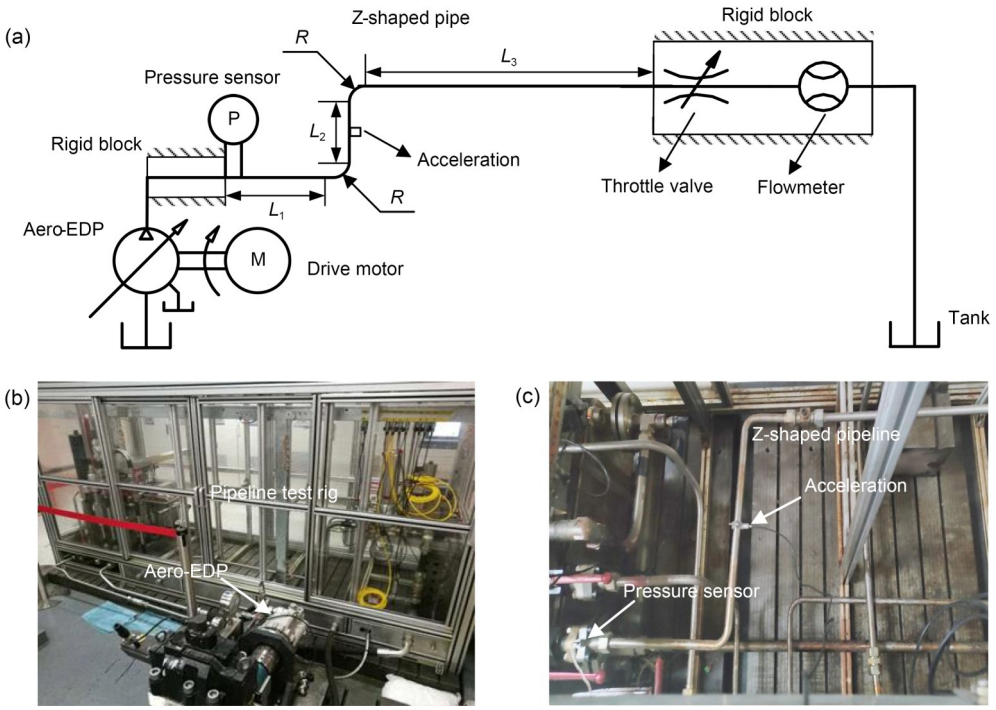

Fig. 13 Schematic of the test rig: (a) hydraulic schematic diagram of the test rig; (b) aero-EDP and pipeline test rig; (c) Z-shaped pipeline and sensors

Table 4 Parameters of hydraulic components and instruments

Equipment	Model type	Parameter	Value
EDP	YZB-56	Rated pressure	28 MPa
		Max displacement	56 mL/r
		Number of pistons	9
Drive motor	Rexroth-A6VM107	Max displacement	107 mL/r
Throttle valve	Hydac-DVP-30-01.X	Nominal pressure	35 MPa
		Max flow rate	300 L/min
Pressure sensor	Kulite-HKM-375(M)	Rated pressure range	0–35 MPa
		Resolution	0.25% FS
		Natural frequency	>400 kHz
Accelerator	CHENGTEC-CT1001L	Sensitivity	10.3 mV/g
		Max acceleration	5000 m/s^2
		Frequency range	1–8000 Hz
Flowmeter	VSE-VS4	Flow rate range	1–300 L/min

FS: full scale

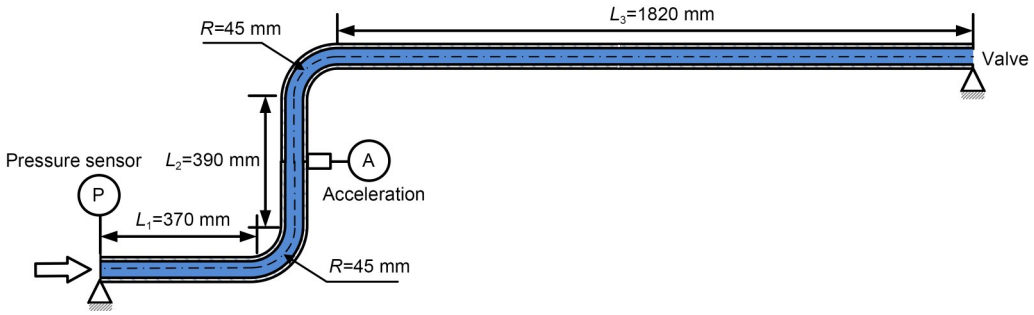

Fig. 14 Layout of the Z-shaped pipeline

Table 5 Material and geometrical properties of the Z-shaped liquid pipe

Item	Parameter	Value
Pipe (steel)	Mass density, ρ_p	7850 kg/m^3
	Young's modulus, E	206 GPa
	Shear modulus, G	65.1 GPa
	Pipe wall thickness, e_p	2 mm
	Inner radius, r	8 mm
	Poisson's ratio, μ	0.29
Fluid (hydraulic oil)	Mass density, ρ_f	831 kg/m^3
	Bulk modulus, K	1.12 GPa

the solution. Considering that the pipe ends were fixed on the rig blocks, the boundary matrices at the inlet of the pipe could be determined as shown in Eqs. (30) and (31). To obtain the magnitude ratio of acceleration to inlet pressure, the unit pressure excitation is used.

$$\boldsymbol{D}_0(s)=\begin{bmatrix}0&1&0&0&0&0&0&0&0&0&0&0&0&0\\0&0&1&0&0&0&0&0&0&0&0&0&0&0\\0&0&0&0&1&0&0&0&0&0&0&0&0&0\\0&0&0&0&0&0&1&0&0&0&0&0&0&0\\0&0&0&0&0&0&0&0&1&0&0&0&0&0\\0&0&0&0&0&0&0&0&0&0&1&0&0&0\\0&0&0&0&0&0&0&0&0&0&0&0&1&0\end{bmatrix}_{7\times 14}, \tag{30}$$

$$\boldsymbol{E}_0(s)=[\,1\quad 0\quad 0\quad 0\quad 0\quad 0\quad 0\,]^{\mathrm{T}}. \tag{31}$$

The boundary matrices for the pipeline outlet are shown in Eqs. (32) and (33).

$$\boldsymbol{D}_L(s)=\begin{bmatrix}-Z_v(s)&1&0&0&0&0&0&0&0&0&0&0&0&0\\0&0&1&0&0&0&0&0&0&0&0&0&0&0\\0&0&0&0&1&0&0&0&0&0&0&0&0&0\\0&0&0&0&0&0&1&0&0&0&0&0&0&0\\0&0&0&0&0&0&0&0&1&0&0&0&0&0\\0&0&0&0&0&0&0&0&0&0&1&0&0&0\\0&0&0&0&0&0&0&0&0&0&0&0&1&0\end{bmatrix}_{7\times 14}, \tag{32}$$

$$\boldsymbol{E}_L(s)=[\,0\quad 0\quad 0\quad 0\quad 0\quad 0\quad 0\,]^{\mathrm{T}}, \tag{33}$$

where $Z_v(s)$ is the fluid impedance of the throttle valve, which can be derived by performing the linearized approximation and Laplace transformation on its flow-pressure characteristic.

The fluid impedance of the throttle valve (Johnston and Edge, 1991) can be described as

$$Z_v(s)=\frac{P_v(s)}{Q_v(s)}=\frac{\sqrt{2\rho_f P_v}}{C_q A_c}=2\frac{P_v}{Q_v}, \tag{34}$$

where Q_v is the flow rate, C_q is the coefficient of the throttle, A_c is the opening area of the valve, and P_v is the pressure drop.

The flow rate of the system was maintained at 30 L/min in the experiment, while the steady pressure remained at 28 MPa. Therefore, the throttling impedance could be calculated with Eq. (34), which is 1.12×10^{11} Pa·s^3/m. The detailed derivation is given in Section S3 of the ESM.

5.3 Experimental results

We conducted a speed-sweep test by varying the pump speed from 1050 r/min to 2900 r/min, with steps of 50 r/min. The acquired experimental data included inlet-pressure measurements and acceleration signals. The sampling rate for data acquisition was set at 1×10^4 samples per second. The data was processed with the fast Fourier transform (FFT) to obtain the frequency response. For instance, the pressure at the pipeline inlet with a pump speed of 1750 r/min is shown in Fig. 15, and the lateral acceleration at the middle of pipe L_2 with the same pump speed is shown in Fig. 16. The frequency spectra are also shown in the figures, while the pump shaft's frequency is not depicted.

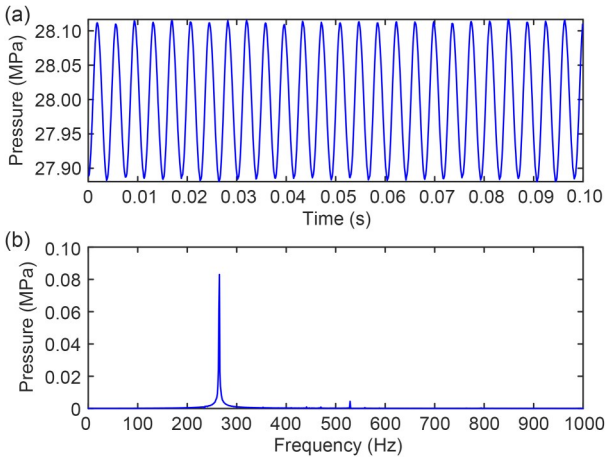

Fig. 15 Pressure at the inlet with a pump speed of 1750 r/min: (a) time-domain measurement; (b) frequency response by FFT

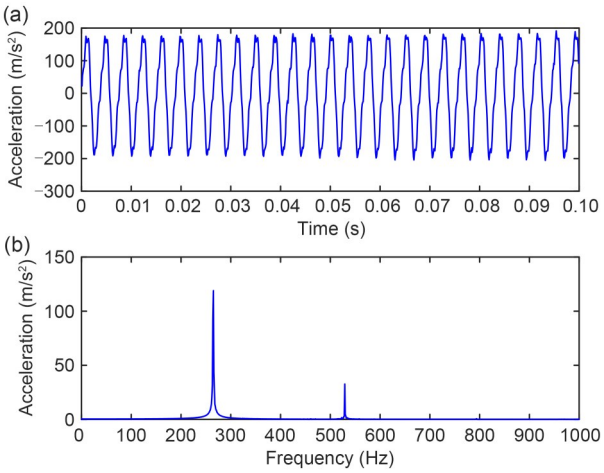

Fig. 16 Lateral acceleration at the middle of pipe L_2 with a pump speed of 1750 r/min: (a) time-domain measurement; (b) frequency response by FFT

The frequency-domain amplitudes of pressure and acceleration, obtained through FFT spanning from 1050 r/min to 2900 r/min, are listed in Table 6.

For the local pipeline in this experiment, the magnitude ratio between acceleration and inlet pressure was selected to verify the accuracy of the FSI model and solution method, which is illustrated in Fig. 17. The resonant frequencies of the improved TMM, FEM, and experimental results are presented in Table 7, demonstrating agreement. All resonant frequencies could be determined and the improved TMM and FEM gave almost the same results. The maximum discrepancy between the predicted resonant frequency in simulation and experimental results was 2.73%, while the minimum discrepancy was 0.31%. Some discrepancies can be attributed to potential differences between simulation settings and practical system conditions, such as pipe connections.

6 Conclusions

The frequency-domain FSI analysis of hydraulic piping systems is studied in this paper. The following conclusions can be drawn:

(1) Considering the complex pipeline for the situation of practical hydraulic systems, the fluid friction and curved pipe's flexibility correction are taken into account in the 14-equation FSI model.

(2) The frequency-domain solution TMM may encounter computational instability when calculating the complex pipes. The reason is probably the ill-conditioned transfer matrices. To address this problem, an improved TMM is proposed in this work, based on pipe's division and matrix stacking technique. The effectiveness is verified with the numerical case of an L-shaped pipe.

Table 6 Frequency response amplitudes obtained by the speed-sweep test

Pump speed (r/min)	Frequency (Hz)	Pressure (MPa)	Acceleration (m/s^2)
1050	159	0.017	0.54
1100	167	0.015	0.67
1150	173	0.020	2.37
1200	182	0.020	96.2
1250	189	0.020	3.31
1300	196	0.025	0.25
1350	204	0.027	2.30
1400	212	0.029	2.02
1450	220	0.046	3.47
1500	227	0.060	8.21
1550	234	0.068	6.43
1600	241	0.059	9.07
1650	249	0.096	22.9
1700	257	0.081	30.3
1750	265	0.083	116
1800	272	0.126	139
1850	279	0.068	60.9
1900	286	0.026	51.6
1950	293	0.008	20.9
2000	301	0.008	16.0
2050	309	0.014	11.8
2100	317	0.018	13.8
2150	324	0.023	117
2200	332	0.022	21.6
2250	339	0.027	23.9
2300	346	0.019	11.3
2350	354	0.025	12.3
2400	361	0.032	6.97
2450	369	0.040	4.28
2500	376	0.049	1.07
2550	384	0.058	3.17
2600	392	0.057	6.42
2650	399	0.057	8.03
2700	406	0.074	19.2
2750	413	0.123	26.4
2800	422	0.176	33.9
2850	428	0.170	36.3
2900	434	0.211	63.9

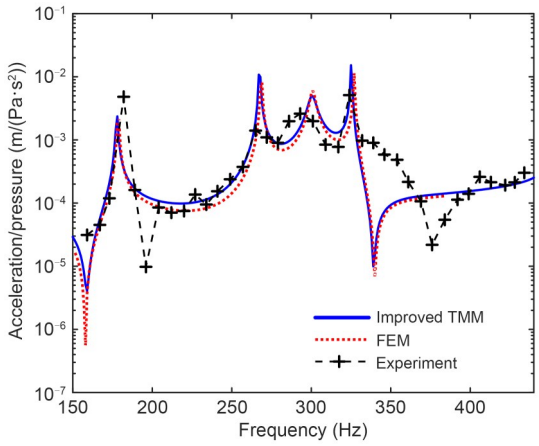

Fig. 17 Magnitude ratio of the lateral acceleration to pressure at inlet obtained by improved TMM, FEM, and experiment

Table 7 Experimental and simulated modal frequencies for the Z-shaped hydraulic pipeline

Experiment frequency (Hz)	Improved TMM		FEM	
	Frequency (Hz)	Error (%)	Frequency (Hz)	Error (%)
182	178	2.20	179	1.65
265	267	0.75	269	1.51
293	301	2.73	301	2.73
324	325	0.31	327	0.93

(3) In the experimental validation, the boundary modeling for the practical hydraulic system, especially for the hydraulic valve, is studied. The magnitude ratio of acceleration to inlet pressure is employed as the index for the validation. Good agreement of experimental and calculated results is achieved, indicating the proposed method is effective and accurate.

The theory in this paper could be beneficial for the vibration prediction and design of the aircraft hydraulic piping system. Further work might involve the improved TMM for more complex pipelines with clamps and supports.

Acknowledgments

This work is supported by the National Natural Science Foundation of China (Nos. 51975025 and 51890822), the Young Elite Scientists Sponsorship Program by China Association for Science and Technology (No. 2016QNRC001), and the National Key Research and Development Program of China (No. 2019YFB2004500). Contribution to the experiment part by Mr. Liandeng WANG (Beihang University, China) is gratefully acknowledged.

Author contributions

Yang DENG: Investigation, Methodology, Validation, Writing–original draft. Zongxia JIAO: Conceptualization, Methodology, Supervision, Writing–reviewing. Yuanzhi XU: Methodology, Supervision, Writing–reviewing and editing.

Conflict of interest

Yang DENG, Zongxia JIAO, and Yuanzhi XU declare that there is no conflict of interest regarding the publication of this article.

References

Brown FT, Tentarelli SC, 2001. Dynamic behavior of complex fluid-filled tubing systems—part 1: tubing analysis. *Journal of Dynamic Systems, Measurement, and Control*, 123(1):71-77. https://doi.org/10.1115/1.1344879

Davidson LC, Smith JE, 1969. Liquid-structure coupling in curved pipes. *The Shock and Vibration Bulletin*, 40(4): 197-207.

Davidson LC, Smith JE, 1972. Liquid-structure coupling in curved pipes–II. *The Shock and Vibration Bulletin*, 43(1): 123-136.

de Jong CAF, 1994. Analysis of Pulsations and Vibrations in Fluid-Filled Pipe Systems. PhD Thesis, Eindhoven University of Technology, Eindhoven, the Netherlands. https://doi.org/10.6100/IR423649

Ferras D, Manso PA, Schleiss AJ, et al., 2018. One-dimensional fluid-structure interaction models in pressurized fluid-filled pipes: a review. *Applied Sciences*, 8(10):1844. https://doi.org/10.3390/app8101844

Gao PX, Zhai JY, Yan YY, et al., 2016. A model reduction approach for the vibration analysis of hydraulic pipeline system in aircraft. *Aerospace Science and Technology*, 49: 144-153. https://doi.org/10.1016/j.ast.2015.12.002

Gao PX, Yu T, Zhang YL, et al., 2021. Vibration analysis and control technologies of hydraulic pipeline system in aircraft: a review. *Chinese Journal of Aeronautics*, 34(4): 83-114. https://doi.org/10.1016/j.cja.2020.07.007

Guo XM, Cao YM, Ma H, et al., 2022a. Dynamic analysis of an L-shaped liquid-filled pipe with interval uncertainty. *International Journal of Mechanical Sciences*, 217:107040. https://doi.org/10.1016/j.ijmecsci.2021.107040

Guo XM, Xiao CL, Ge H, et al., 2022b. Dynamic modeling and experimental study of a complex fluid-conveying pipeline system with series and parallel structures. *Applied Mathematical Modelling*, 109:186-208. https://doi.org/10.1016/j.apm.2022.04.003

Guo XM, Xiao CL, Ma H, et al., 2022c. Improved frequency modeling and solution for parallel liquid-filled pipes considering both fluid-structure interaction and structural coupling. *Applied Mathematics and Mechanics*, 43(8):1269-1288. https://doi.org/10.1007/s10483-022-2883-9.

Guo XM, Cao YM, Ma H, et al., 2022d. Vibration analysis for a parallel fluid-filled pipelines-casing model considering casing flexibility. *International Journal of Mechanical*

Sciences, 231:107606.
https://doi.org/10.1016/j.ijmecsci.2022.107606

Guo XM, Ge H, Xiao CL, et al., 2022e. Vibration transmission characteristics analysis of the parallel fluid-conveying pipes system: numerical and experimental studies. *Mechanical Systems and Signal Processing*, 177:109180.
https://doi.org/10.1016/j.ymssp.2022.109180

Guo XM, Gao PX, Ma H, et al., 2023. Vibration characteristics analysis of fluid-conveying pipes concurrently subjected to base excitation and pulsation excitation. *Mechanical Systems and Signal Processing*, 189:110086.
https://doi.org/10.1016/j.ymssp.2022.110086

Ji WH, Sun W, Du DX, et al., 2023. Dynamics modeling and stress response solution for liquid-filled pipe system considering both fluid velocity and pressure fluctuations. *Thin-Walled Structures*, 188:110831.
https://doi.org/10.1016/j.tws.2023.110831

Jiao ZX, Hua Q, Yu K, 1999. Frequency domain analysis of vibrations in liquid filled piping systems. *Acta Aeronautica et Astronautica Sinica*, 20(4):316-320 (in Chinese).
https://doi.org/10.3321/j.issn:1000-6893.1999.04.007

Johnston DN, Edge KA, 1991. The impedance characteristics of fluid power components: restrictor and flow control valves. *Proceedings of the Institution of Mechanical Engineers, Part I: Journal of Systems and Control Engineering*, 205(1):3-10.
https://doi.org/10.1243/PIME_PROC_1991_205_308_02

Kwong AHM, Edge KA, 1996. Structure-borne noise prediction in liquid-conveying pipe systems. *Proceedings of the Institution of Mechanical Engineers, Part I: Journal of Systems and Control Engineering*, 210(3):189-200.
https://doi.org/10.1243/PIME_PROC_1996_210_454_02

Lesmez MW, Wiggert DC, Hatfield FJ, 1990. Modal analysis of vibrations in liquid-filled piping systems. *Journal of Fluids Engineering*, 112(3):311-318.
https://doi.org/10.1115/1.2909406

Li QS, Yang K, Zhang LX, et al., 2002. Frequency domain analysis of fluid-structure interaction in liquid-filled pipe systems by transfer matrix method. *International Journal of Mechanical Sciences*, 44(10):2067-2087.
https://doi.org/10.1016/S0020-7403(02)00170-4

Li SJ, Liu GM, Kong WT, 2014. Vibration analysis of pipes conveying fluid by transfer matrix method. *Nuclear Engineering and Design*, 266:78-88.
https://doi.org/10.1016/j.nucengdes.2013.10.028

Li SJ, Karney BW, Liu GM, 2015. FSI research in pipeline systems–a review of the literature. *Journal of Fluids and Structures*, 57:277-297.
https://dx.doi.org/10.1016/j.jfluidstructs.2015.06.020

Li X, Li WH, Shi J, et al., 2022. Pipelines vibration analysis and control based on clamps' locations optimization of multi-pump system. *Chinese Journal of Aeronautics*, 35(6):352-366.
https://doi.org/10.1016/j.cja.2021.04.010

Liu GM, Li YH, 2011. Vibration analysis of liquid-filled pipelines with elastic constraints. *Journal of Sound and Vibration*, 330(13):3166-3181.
https://doi.org/10.1016/j.jsv.2011.01.022

Ouyang XP, Gao F, Yang HY, et al., 2012a. Modal analysis of the aircraft hydraulic-system pipeline. *Journal of Aircraft*, 49(4):1168-1174.
https://doi.org/10.2514/1.C031660

Ouyang XP, Gao F, Yang HY, et al., 2012b. Two-dimensional stress analysis of the aircraft hydraulic system pipeline. *Proceedings of the Institution of Mechanical Engineers, Part G: Journal of Aerospace Engineering*, 226(6):532-539.
https://doi.org/10.1177/0954410011413011

Pardue TE, Vigness I, 1951. Properties of thin-walled curved tubes of short-bend radius. *Journal of Fluids Engineering*, 73(1):77-84.
https://doi.org/10.1115/1.4016146

Skalak R, 1956. An extension of the theory of water hammer. *Journal of Fluids Engineering*, 78(1):105-115.
https://doi.org/10.1115/1.4013579

Tentarelli SC, Brown FT, 2001. Dynamic behavior of complex fluid-filled tubing systems—part 2: system analysis. *Journal of Dynamic Systems, Measurement, and Control*, 123(1):78-84.
https://doi.org/10.1115/1.1344882

Tijsseling AS, 1996. Fluid-structure interaction in liquid-filled pipe systems: a review. *Journal of Fluids and Structures*, 10(2):109-146.
https://doi.org/10.1006/jfls.1996.0009

Tijsseling AS, 2019. An overview of fluid-structure interaction experiments in single-elbow pipe systems. *Journal of Zhejiang University-SCIENCE A (Applied Physics & Engineering)*, 20(4):233-242.
https://doi.org/10.1631/jzus.A1800564

Vigness I, 1943. Elastic properties of curved tubes. *Journal of Fluids Engineering*, 65(2):105-117.
https://doi.org/10.1115/1.4018692

Wang SP, Tomovi M, Liu H, 2015. Commercial Aircraft Hydraulic Systems. Shanghai Jiao Tong University Press, Shanghai, China, p.53-60.

Wiggert DC, Tijsseling AS, 2001. Fluid transients and fluid-structure interaction in flexible liquid-filled piping. *Applied Mechanics Reviews*, 54(5):455-481.
https://doi.org/10.1115/1.1404122

Wiggert DC, Hatfield FJ, Stuckenbruck S, 1987. Analysis of liquid and structural transients in piping by the method of characteristics. *Journal of Fluids Engineering*, 109(2):161-165.
https://doi.org/10.1115/1.3242638

Xu YZ, Johnston DN, Jiao ZX, et al., 2014. Frequency modelling and solution of fluid-structure interaction in complex pipelines. *Journal of Sound and Vibration*, 333(10):2800-2822.
https://doi.org/10.1016/j.jsv.2013.12.023

Yang K, Li QS, Zhang LX, 2004. Longitudinal vibration analysis of multi-span liquid-filled pipelines with rigid constraints. *Journal of Sound and Vibration*, 273(1-2):125-147.
https://doi.org/10.1016/S0022-460X(03)00422-X

Zhang L, Tijsseling SA, Vardy EA, 1999. FSI analysis of liquid-filled pipes. *Journal of Sound and Vibration*, 224(1):69-99.
https://doi.org/10.1006/jsvi.1999.2158

Zielke W, 1968. Frequency-dependent friction in transient pipe flow. *Journal of Basic Engineering*, 90(1):109-115.
https://doi.org/10.1115/1.3605049

Electronic supplementary materials

Sections S1–S3